Using a Grid-Based Filter to Solve InSAR Phase Unwrapping

Juan J. Martinez-Espla, Tomas Martinez-Marin, and Juan M. Lopez-Sanchez, *Senior Member, IEEE*

***Abstract*—This letter presents a phase-unwrapping (PU) algorithm for synthetic aperture radar interferometry based on a grid-based filter. The proposed PU algorithm, which is based on state-space techniques, simultaneously performs noise filtering and PU. The formulation of this technique provides independence from noise statistics and is not constrained by the nonlinearity of the problem. Results obtained with synthetic data show a significant improvement with respect to other conventional PU algorithms in some situations.**

***Index Terms*—Extended Kalman filter (EKF), grid filter, particle filter, phase unwrapping (PU), synthetic aperture radar interferometry.**

I. Introduction

PHASE unwrapping (PU) is one of the key processing steps in all applications of synthetic aperture radar (SAR) interferometry. A lot of literature concerning different techniques to solve the PU problem has been published during the last years. We refer to the book by Ghiglia and Pritt [1] for an excellent overview. There are two general types of conventional PU methods. The algorithms of the first group, which are generally named path-following or region-growing algorithms, isolate and/or mask problematic zones containing residues and unwrap the interferogram by avoiding these zones. The techniques of the second group provide a global solution which minimizes a cost function over the whole interferogram. Some of these techniques, and other alternative approaches which do not correspond to these groups, make use of a prefiltering stage before starting the unwrapping procedure with the filtered phase, for instance [2]. Consequences of these strategies are the following: phase information in noisy pixels is not recovered by the path-following algorithms, noisy pixels distort the solution in global approaches, thus affecting the noise-free areas, and the information contained in noisy pixels is lost if a prefiltering stage is carried out.

There exists another group of statistical solutions for PU. They are known as "multichannel" techniques because they require multiple acquisitions (not only two images) to be applied. In contrast, our approach is devised for conventional "single-channel" interferometry, i.e., for a single interferogram obtained with only one pair of images.

Manuscript received September 8, 2006; revised September 13, 2007. This work was supported in part by the Spanish Ministry of Education and Science (MEC) under Project TEC2005-06863-C02-02 and in part by the Generalitat Valenciana under Project ACOMP07/087.

The authors are with the Departamento de Física, Ingeniería de Sistemas y Teoría de la Señal, Universidad de Alicante, 03080 Alicante, Spain (e-mail: jjme1@alu.ua.es; tomas@dfists.ua.es; juanma-lopez@ieee.org).

Digital Object Identifier 10.1109/LGRS.2008.915734

The algorithm proposed by Ferretti *et al.* [3] makes use of a set of images acquired with the same sensor, but the interferograms generated by combining these images exhibit different baselines. Since the influence of different error contributions is a function of the baseline, this algorithm exploits the sensitivity/insensitivity to the baseline for minimizing the total error by properly using all the information. The algorithms presented by Ferraiuolo *et al.* [4] and Fornaro *et al.* [5] are designed for multifrequency systems, i.e., for the combination of interferograms generated with images acquired at several frequency bands. Again, the sensitivity of errors to the different scales provided by different wavelengths is exploited statistically to derive a better global solution.

Multichannel techniques have the advantage to eliminate, or at least mitigate, the ambiguity problem related to the wrapping operator. However, they have the drawback to amplify the noise contribution during the process for ambiguity reduction. This effect is more important when the noise contribution is large (i.e., small values of coherence γ) and the ambiguity reduction factor d is large too ($d \gg 1$), introducing large spikes (impulsive noise). In the particular case of the PU algorithm proposed by Fornaro *et al.* [5], error propagation is a key factor.

We are interested in recovering as much information as possible from the interferogram, including the noisy pixels. Therefore, an ideal method would consider every pixel to be simultaneously unwrapped and filtered.

There exists an algorithm that shares the same objective and was already published in [6]–[10]. That algorithm combines a slope estimator with an extended Kalman filter (EKF), showing the mentioned feature of integrating a slope/frequency estimator and an EKF in an elegant fashion to simultaneously achieve noise reduction and PU. Unfortunately, that solution is founded on the following two assumptions. First, both the evolution and measurement models are available and correspond to the linear functions. Second, the noise affecting both the evolution and measurement stages is Gaussian. When the constraint of Gaussian noise holds but the models are not linear functions, the EKF has been used in many cases as a good solution that approximates the nonlinearities by local linearizations. The main problem arises when the noise present in the interferogram is not Gaussian. The EKF cannot guarantee a successful PU, as we will show later with an example.

In this letter, we propose to substitute the EKF by a grid-based filter (GbF), which is not subject to any linear or Gaussian constraints. A detailed tutorial about different methods to broach nonlinear/non-Gaussian problems can be found in [11]. The solution proposed in this letter combines a GbF with a phase slope estimator to simultaneously unwrap and

filter the interferometric phase. Although this approach could be combined with path-following strategies to enhance their performance with the embedded noise filtering, we present here the algorithm without any conditioned scheme for choosing the unwrapping path. In particular, the basic algorithm introduced in this letter runs the interferogram row by row, passing through zones of low coherence and containing residues, unwrapping and filtering the phase at the same time. We refer to [1] for the definition of coherence and residues.

This letter is organized as follows. Section II introduces the basic formulation of the PU problem. The GbF formulation for solving the PU is presented in Section III. Then, Section IV illustrates the performance of the new method with an example using a data set extracted from the book by Ghiglia and Pritt [1]. A comparison with both the Goldstein branch-cut algorithm [1] and the cited EKF approach is also discussed. Finally, conclusions are drawn in Section V.

II. PU Basic Formulation

By assuming a 1-D notation, for the complex coherence between two SAR images γ, we have, in polar notation, at pixel k

$$\gamma(k) = a(k) \cdot \exp\left[j \cdot \tilde{\varphi}(k)\right] \tag{1}$$

where $a(k)$ is the observed interferometric coherence (between zero and one), and $\tilde{\varphi}(k)$ is the modulo 2π mapped interferometric phase, which is also called wrapped phase. This mapping can be expressed by

$$\begin{aligned}\tilde{\varphi}(k) &= \lfloor \varphi(k) + \tilde{e}_{\varphi}(k) \rfloor_{|2\pi} \\ &= \varphi(k) + \tilde{e}_{\varphi}(k) \pm n \cdot 2\pi \in (-\pi, \pi]\end{aligned} \tag{2}$$

where $\varphi(k)$ is the true unambiguous absolute phase at pixel k, and $\tilde{e}_{\varphi}(k)$ is the mapped phase error at pixel k.

The final objective is to obtain the unwrapped or absolute phase $\varphi(k)$ from the noisy 2π mapped phases $\tilde{\varphi}(k)$ contained in the interferogram. At this step, we will be interested in the calculus of the phase difference from one pixel to the next

$$\tilde{\Delta}_{\varphi}(k) = \left[\tilde{\varphi}(k+1) - \tilde{\varphi}(k)\right]_{|2\pi} \tag{3}$$

that yields

$$\tilde{\Delta}_{\varphi}(k) = \left\lfloor \delta_{\varphi}(k) + \left[\tilde{e}_{\varphi}(k+1) - \tilde{e}_{\varphi}(k)\right]_{|2\pi} \right\rfloor_{|2\pi} \tag{4}$$

where $\delta_{\varphi}(k)$ is the true discrete phase derivative, and its modulus is always supposed to be smaller than π (i.e., there is no aliasing).

Finally, the unwrapped phase $\varphi(k)$ can be obtained through the recursive expression

$$\varphi(k+1) = \varphi(k) + \tilde{\Delta}_{\varphi}(k). \tag{5}$$

III. Approximated GbF

A. Introduction to the GbF

From now on, to be coherent with the notation of state-space methods, the unwrapped phase at pixel k, i.e., $\varphi(k)$, will be referred to as the corresponding state x_k at pixel k. The concept of state, which is also known as cell, is introduced next.

The objective is to calculate estimates of the state x_k based on the set of all available observations $z_{1:k} = \{z_i, i = 1, \ldots, k\}$ up to pixel k. Thus, the filter tries to approximate the posterior probability density function (pdf) $p(x_k|z_{1:k})$. By considering the Markovian assumption, the pdf $p(x_k|z_{1:k})$ can be obtained recursively from the pdf $p(x_{k-1}|z_{1:k-1})$ calculated at the previous pixel $k-1$. It is supposed that the initial pdf $p(x_0|z_0) \equiv p(x_0)$ is known. Then, this sequential problem is divided into two stages: prediction and update. The prediction stage is solved by employing the evolution model, and the update stage is solved by the observation model. It is assumed that both models are known.

For a grid-based approximation, it is assumed that some necessary information is available.

1) Initial weight distribution: $w_{\mathrm{o}}^i, i = 1, \ldots, N_{\mathrm{s}}$, where N_{s} is the number of cells (see cell definition). An initial state x_{o} is also selected from this distribution according to any criteria, for instance, the average value or the state whose weight is maximum.
2) Observations: $z_1, \ldots, z_T$, where $z_k, k = 1, \ldots, T$, is the observed wrapped noisy phase at pixel k, which is formerly denoted as $\tilde{\varphi}(k)$, and T is the total number of pixels.
3) Evolution model: $x_k = f_k(x_{k-1}) \leftrightarrow p(x_k|x_{k-1})$.
4) Observation model: $z_k = h_k(x_k) \leftrightarrow p(z_k|x_k)$.

The state space of our interferometric problem is continuous but can be decomposed into a discrete state space; thus, this suboptimal solution can be adopted. Specifically, the continuous state space is divided into N_{s} cells or states $\{x_k^i, i = 1, \ldots, N_{\mathrm{s}}\}$ which correspond to all possible phase values. The grid must be sufficiently dense to get a good approximation to the continuous state space. It is assumed that the pdf at pixel $k-1$ can be approximated as

$$p(x_{k-1}|z_{1:k-1}) \approx \sum_{i=1}^{N_{\mathrm{s}}} w_{k-1|k-1}^i \delta\left(x_{k-1} - x_{k-1}^i\right) \tag{6}$$

where $w_{k-1|k-1}^i = p(x_{k-1} = x_{k-1}^i|z_{1:k-1})$ is a weight that represents the conditional probability of x_{k-1}^i given observations up to pixel $k-1$.

Then, the prediction equation and the corresponding weight estimation are, respectively, given by

$$p(x_k|z_{1:k-1}) \approx \sum_{i=1}^{N_{\mathrm{s}}} w_{k|k-1}^i \delta\left(x_k - x_k^i\right) \tag{7}$$

$$w_{k|k-1}^i \approx \sum_{j=1}^{N_{\mathrm{s}}} w_{k-1|k-1}^j p\left(\bar{x}_k^i|\bar{x}_{k-1}^j\right) \tag{8}$$

where $\delta()$ represents the Dirac Delta.

The subscript $1:k-1$ in the left side of (7) means that x_k depends on all observations $z_1, z_2, \ldots, z_{k-1}$. The subscript $k-1|k-1$ in the right side of (8) indicates that the weight is estimated at pixel $k-1$, taking into account the observations up to $k-1$. In contrast, $w^i_{k|k-1}$, which is obtained after the prediction stage, indicates that the weight is estimated at pixel k, considering the observations up to $k-1$ (8). As previously introduced, the assumption of the first-order Markovian process allows the following simplification: $p(x_k|x_{k-1}, z_{1:k-1}) = p(x_k|x_{k-1})$. In this way, if $w^i_{k-1|k-1}$ is known, it is possible to calculate $w^i_{k|k-1}$ through the evolution model $p(x_k|x_{k-1})$ by using (8).

The update equation and the corresponding weight estimation are given by

$$p(x_k|z_{1:k}) \approx \sum_{i=1}^{N_s} w^i_{k|k}\delta\left(x_k - x^i_k\right) \tag{9}$$

$$w^i_{k|k} \approx \frac{w^i_{k|k-1}p\left(z_k|\bar{x}^i_k\right)}{\sum_{j=1}^{N_s} w^j_{k|k-1}p\left(z_k|\bar{x}^j_k\right)}. \tag{10}$$

In this stage, the observation at pixel k is included when determining $w^i_{k|k}$ (10). Every weight $w^i_{k|k}$ is computed at the center of the corresponding cell $\bar{x}^i_k$. The probabilities $p(\bar{x}^i_k|\bar{x}^j_{k-1})$ and $p(z_k|\bar{x}^i_k)$ are defined by the evolution and observation models at pixel k, which are given by

$$\bar{x}^i_k = \bar{x}^j_{k-1} + \Delta\hat{\varphi}_{k-1} + n_{k-1} \tag{11}$$

$$z_k = \bar{x}^i_k + \nu_k \tag{12}$$

where $\Delta\hat{\varphi}_{k-1}$ represents a phase slope estimation, and n_k and ν_k are supposed to be approximate models for the noise present in both the evolution and measurement stages, respectively. Several techniques can be used to obtain an estimation of the phase slope. For instance, the mode of the power spectral density was used in [6] and [7] due to its supposed insensitiveness and robustness to superimposed white noise, whereas a matrix-pencil approach and a slope average-based method were proposed in [12] and [13], respectively. All of them are perfectly applicable. The first one has been selected in this case for the sake of comparison. It is well known that the noise present in an interferogram is Wishart. Therefore, noise ν_k has been modeled as a Wishart discrete distribution. Concerning n_k, it models the uncertainty introduced by the slope estimator (based on the power spectral density in this letter). It has been modeled as a Gaussian discrete distribution for the sake of comparison with [6] and [7].

If an EKF is used, instead of the GbF, a possible solution (presented in [6]–[10]) employed two dimensions per pixel (inphase and quadrature components of phase contained in the InSAR image), thus increasing complexity. The update equation was as follows:

$$x_k = x^p_k + K \cdot (z_k - x^p_k) \tag{13}$$

where z_k is the measurement, x^p_k is the unwrapped phase obtained by the prediction equation of the EKF, K is the Kalman gain, and x_k is the unwrapped solution obtained by the update and final equation [14]. It can be demonstrated that

$$|\max\left[K \cdot (z_k - x^p_k)\right]| = 1\,\text{rad} \tag{14}$$

which means that a very bad prediction x^p_k provided by an erroneous slope estimation only can be corrected up to ± 1 rad by the update equation in the best case.

In contrast, the application of a GbF solution is more straightforward, with the great advantage of using only one dimension per pixel (directly the phase), bringing down the complexity to its simplest case, and it does not show the mentioned restriction in the update equation.

A priori, one drawback of the grid-based methods could be the constraint of a finite state space, but this is not the case in the interferometric PU problem. The grid-based solution that we propose here makes use of a sliding window W^s_k to cover the complete state space. This window is 2π wide and is centered in the previous value for the unwrapped phase given by GbF_{av}, which is introduced next. It is based on the assumption that the phase difference between two contiguous pixels must be contained in the interval $(-\pi, +\pi]$. In this way, this sliding state space allows us to afford the interferometric PU problem independently of the width of the complete state space. Computational cost increases linearly with N_s—the number of cells.

B. Two-Dimensional PU Algorithm

To extend the use of GbF to 2-D interferograms, any prediction estimate will be calculated depending on two neighbors so that only the stage concerning the evolution model (7) needs to be modified as follows

$$w^i_{k|k-1} \approx \frac{1}{2} \cdot \left(\sum_{j=1}^{N_s} w^j_{k-1|k-1} \cdot p_{\text{H}}\left(\bar{x}^i_k|\bar{x}^j_{k-1}\right) + \sum_{j=1}^{N_s} w^j_{k-m|k-m} \cdot p_{\text{V}}\left(\bar{x}^i_k|\bar{x}^j_{k-m}\right) \right) \tag{15}$$

where $w^j_{k-1|k-1}$ is the final weight distribution after the update stage at pixel $k-1$, and $p_{\text{H}}(\bar{x}^i_k|\bar{x}^j_{k-1})$ is the evolution model in the horizontal direction, also at pixel $k-1$, which is given by

$$\bar{x}^i_k = \bar{x}^j_{k-1} + \Delta\hat{\varphi}^{\text{H}}_{k-1} + n^{\text{H}}_{k-1} \tag{16}$$

where $\bar{x}^j_{k-1}$ refers to the unwrapped phase at pixel $k-1$, $\Delta\hat{\varphi}^{\text{H}}_{k-1}$ refers to the horizontal slope estimation at pixel $k-1$, and n^{H}_{k-1} refers to the Gaussian-noise sample at pixel $k-1$. Note that pixel $k-1$ is the previously unwrapped one that is placed in the same row and adjacent to the current pixel k.

On the other hand, $w^j_{k-m|k-m}$ is the final weight distribution after the update stage at pixel $k-m$, and $p_{\text{V}}(\bar{x}^i_k|\bar{x}^j_{k-m})$ is the

Algorithm: Grid-based Filter Phase Unwrapping

- Initial weight distribution: w_o^i; $i=1,...,N_s$. An initial state x_o is selected.

FOR $k = 0,...,T$
- Sliding window update: W_k^s
- Phase slope estimations $\Delta\hat{\varphi}_H$ and $\Delta\hat{\varphi}_V$

FOR $i = 1,...,N_s$:
- Assign the weight $w^i_{k|k-1}$ according to (8)

END FOR

- Normalize: $w^i_{k|k-1}$

FOR $i = 1,...,N_s$:
- Assign the weight $w^i_{k|k}$ according to (10)

END FOR

- Normalize: $w^i_{k|k}$
- Unwrapped phase (two possible solutions):
  - Cell whose weight is maximum: $\bar{x}_k = \tilde{x}_k^i\,|_{\max\left(w^i_{k|k}\right)}$
  - Weighted average: $\bar{x}_k = \sum_{i=1}^{N_s} w^i_{k|k} \cdot \tilde{x}_k^i$

END FOR

Fig. 1. Pseudocode of the PU algorithm using a GbF.

evolution model in the vertical direction, also at pixel $k-m$, which is given by

$$\bar{x}_k^i = \bar{x}_{k-m}^j + \Delta\hat{\varphi}_{k-m}^{\mathrm{V}} + r_{k-m}^{\mathrm{V}} \tag{17}$$

where $\bar{x}_{k-m}^j$ refers to the unwrapped phase at pixel $k-m$, $\Delta\hat{\varphi}_{k-m}^{\mathrm{V}}$ refers to the vertical slope estimation at pixel $k-m$, and r_{k-m}^{V} refers to the Gaussian-noise sample at pixel $k-m$. Note that pixel $k-m$ is the previously unwrapped one that is placed in the same column and adjacent to the current pixel k.

Finally, a pseudocode of the PU algorithm is shown in Fig. 1.

IV. Results

The results in this section illustrate the performance of different PU solutions as well as the influence of the noisy input signal. The PU solutions are the following: the branch-cut algorithm proposed by Goldstein [1], two approaches of the GbF proposed in this letter, and the EKF algorithm [6]–[10]. The two GbF options consist of selecting the state whose weight is the maximum $\mathrm{GbF_{mx}}$ or selecting the average state of the distribution $\mathrm{GbF_{av}}$. These algorithms have been applied against one example that most of the methods introduced in [1] fail to unwrap: a synthetic interferogram from a mountainous terrain around Long's Peak, Colorado (Fig. 2). The data set, as detailed in [1], is generated with a high-fidelity IFSAR simulator by employing digital terrain elevation models from the U.S. Geological Survey. We have also chosen this synthetic example because the true unwrapped phase is available; thus, one can compare with the phase delivered by the PU algorithms. Although more expensive than other techniques, the computational cost was only a few seconds to unwrap the area shown in Fig. 2(d).

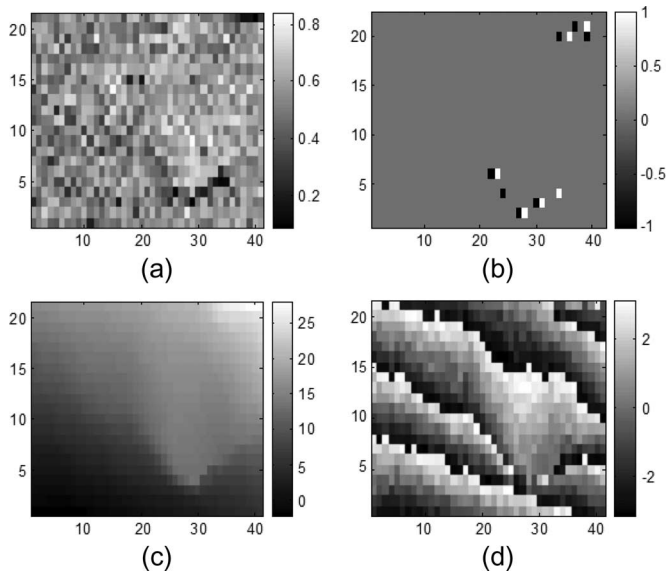

Fig. 2. (a) Coherence. (b) Residues. (c) Ideal unwrapped phase. (d) Noisy input signal.

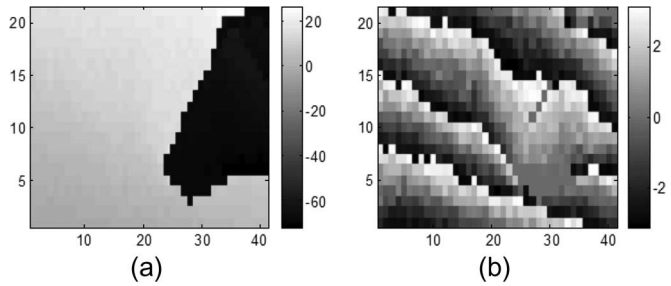

Fig. 3. (a) Goldstein unwrapped phase. (b) Goldstein rewrapped phase.

In the study area, there exist zones where the coherence of data is very poor, for instance, in the surroundings of rows 3–5 and columns 25–35, reaching values lower than 0.3. As a consequence, residues appear.

The PU algorithm proposed by Goldstein [1] identifies the residues and defines the so-called branch cuts between them, which will not be crossed by the unwrapping paths. Note that this method attempts to minimize the branch-cut lengths. As a result, many areas can be completely isolated and, consequently, not be unwrapped consistently with the rest of the interferogram. This is the case shown in Fig. 3.

As observed in Fig. 4 for the same test interferogram, both GbF solutions, namely, $\mathrm{GbF_{mx}}$ and $\mathrm{GbF_{av}}$, can deal with non-Gaussian distributions, in this case Wishart noise, and can recover from errors. This is possible since, as introduced before, they do not need Gaussianity and linearity requirements to be held. Moreover, a GbF solution is able to reach a correction of up to $\pm 2\pi$ rad when compared with the EKF in Fig. 5.

From the comparison of both GbF solutions, it can be concluded that the $\mathrm{GbF_{av}}$ case is more likely to produce smoother profiles than the $\mathrm{GbF_{mx}}$ solution. This feature can be considered as a simultaneous filtering process.

As an additional test, which is not included here due to space constraints, we have computed the difference between the unwrapped results and the original interferogram. The rewrapping

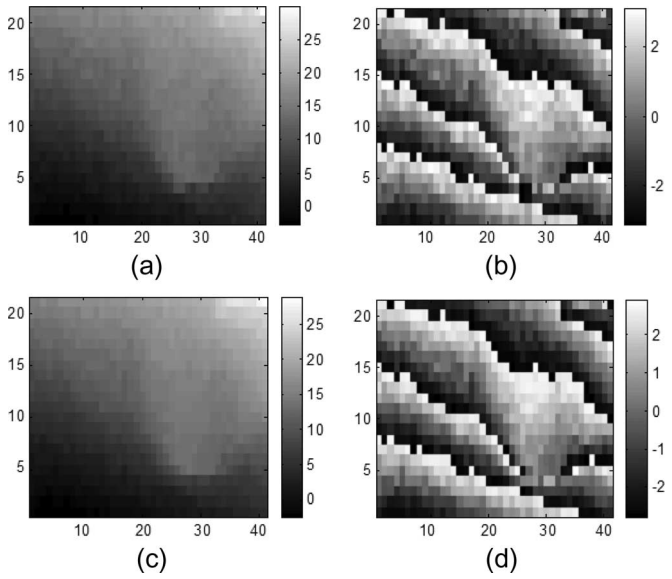

Fig. 4. (a) $\mathrm{GbF}_{\mathrm{mx}}$ unwrapped phase. (b) $\mathrm{GbF}_{\mathrm{mx}}$ rewrapped phase. (c) $\mathrm{GbF}_{\mathrm{av}}$ unwrapped phase. (d) $\mathrm{GbF}_{\mathrm{av}}$ rewrapped phase. The continuous space contained inside the 2π sliding window has been translated into a discrete state space composed of $N = 100$ cells.

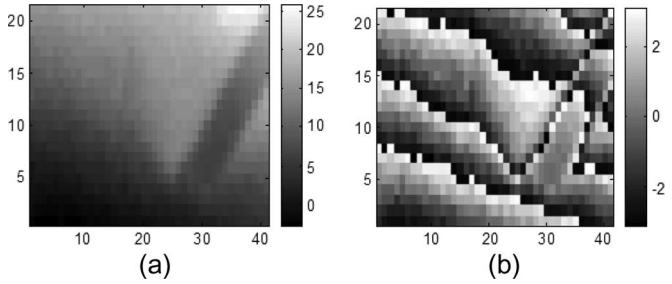

Fig. 5. (a) EKF unwrapped phase. (b) EKF rewrapped phase.

of the GbF results is a noisy constant as expected, and no bias has appeared even for large-size images.

V. Conclusion

A new solution of the PU problem in SAR interferometry is presented in this letter. This solution is based on an approximate GbF. It has been shown that this performs better than the other conventional methods in some situations since the GbF can deal with zones containing residues.

Two variants of this method have been also compared against the EKF method, which shares the same philosophy of simultaneously filtering and unwrapping. These algorithms have been applied to an illustrative example extracted from [1]. It has been shown that, whereas the EKF fails and never recovers, the grid-based solutions perform better and are also able to recover from errors.

Our research lines at present and in the near future are focused on two main issues. First, utilization of other slope estimators, for instance, the matrix-pencil approach proposed in [12] or the slope average-based method introduced in [13]. Second, the combination of the GbF approach with path-following techniques will be analyzed since a better performance is expected from the synergy between both strategies. Moreover, a complete analysis about the performance of this algorithm in different scenarios is currently being carried out.

References

[1] D. C. Ghiglia and M. D. Pritt, *Two-Dimensional Phase Unwrapping. Theory, Algorithms and Software*. New York: Wiley, 1998.

[2] D. Meng, V. Sethu, E. Ambikairajah, and L. Ge, "A novel technique for noise reduction in InSAR images," *IEEE Geosci. Remote Sens. Lett.*, vol. 4, no. 2, pp. 226–230, Apr. 2007.

[3] A. Ferretti, A. Monti Guarnieri, C. Prati, and F. Rocca, "Multi baseline interferometric techniques and applications," in *Proc. ESA Workshop Appl. ERS SAR Interferometry (FRINGE)*, Zurich, Switzerland, Oct. 1996. [Online]. Available: http://www.geo.unizh.ch/rsl/fringe96/papers/ferretti-et-al/

[4] G. Ferraiuolo, V. Pascazio, and G. Schirinzi, "Maximum a *posteriori* estimation of height profiles in InSAR imaging," *IEEE Geosci. Remote Sens. Lett.*, vol. 1, no. 2, pp. 66–70, Apr. 2004.

[5] G. Fornaro, A. Pauciullo, and E. Sansosti, "Phase difference-based multichannel phase unwrapping," *IEEE Trans. Image Process.*, vol. 14, no. 7, pp. 960–972, Jul. 2005.

[6] R. Krämer and O. Loffeld, "Presentation of an improved phase unwrapping algorithm based on Kalman filters combined with local slope estimation," in *Proc. ESA Workshop Appl. ERS SAR Interferometry (FRINGE)*, Zurich, Switzerland, Oct. 1996. [Online]. Available: www.geo.unizh.ch/rsl/fringe96

[7] O. Loffeld and R. Krämer, "Phase unwrapping for SAR interferometry—A data fusion approach by Kalman filtering," in *Proc. IGARSS*, Hamburg, Germany, 1999, pp. 1715–1717.

[8] O. Loffeld and R. Krämer, "Phase unwrapping for SAR interferometry," in *Proc. IGARSS*, Pasadena, CA, 1994, pp. 2282–2284.

[9] O. Loffeld, C. Arndt, and A. Hein, "Estimating the derivative of modulo-mapped phases," in *Proc. ESA Workshop Appl. ERS SAR Interferometry (FRINGE)*, Zurich, Switzerland, Oct. 1996. [Online]. Available: www.geo.unizh.ch/rsl/fringe96

[10] O. Loffeld, "Demodulation of noisy phase or frequency modulated signals with Kalman filters," in *Proc. IEEE Int. Conf. Acoust., Speech Signal Process.*, Adelaide, Australia, 1994, pp. IV-177–IV-180.

[11] M. S. Arulampalam, S. Maskell, N. Gordon, and T. Clapp, "A tutorial on particle filters for online nonlinear/non-Gaussian Bayesian tracking," *IEEE Trans. Signal Process.*, vol. 50, no. 2, pp. 174–188, Feb. 2002.

[12] G. Nico and J. Fortuny, "Using the matrix pencil method to solve phase unwrapping," *IEEE Trans. Signal Process.*, vol. 51, no. 3, pp. 880–886, Mar. 2003.

[13] W. Xu and I. Cumming, "A region-growing algorithm for InSAR phase unwrapping," *IEEE Trans. Geosci. Remote Sens.*, vol. 37, no. 1, pp. 124–134, Jan. 1999.

[14] G. Welch and G. Bishop, "An Introduction to the Kalman Filter," Univ. North Carolina, Chapel Hill, NC, Tech. Rep. 95-041, Feb. 8, 2001.